

AN EXPERIMENTAL INVESTIGATION OF SPIN-UP FROM REST OF A STRATIFIED FLUID

JAN BERT FLOR^{a,*}, JOHN W.M. BUSH^b and MARIUS UNGARISH^c

^aLaboratoire des Écoulements Géophysiques et Industriels (LEGI),
CNRS-INPG-UJF, Grenoble, France; ^bDepartment of Mathematics, MIT, Cambridge, USA;
^cDepartment of Computer Science, Technion, Haifa, Israel

(Received 22 September 2003; In final form 15 March 2004)

We examine the spin-up from rest of a stratified fluid with initial Brunt–Väisälä frequency N bound within a cylindrical container of height $2H$ and radius R which is set to rotate impulsively with angular speed $f/2$. Particular attention is given to characterizing the dependence of the form of the resulting flow on the governing parameters. Our experimental study reveals a wealth of flow behaviours and instabilities. In all experiments, the initial phase of motion is marked by the establishment of mixed axisymmetric corner regions fed by radial Ekman transport, a process detailed in Flór *et al.* (Flór, J.B., Ungarish, M. and Bush, J.W.M., “Spin-up from rest of a stratified fluid: boundary flows”, *J. Fluid Mech.*, **472**, 51–82 (2002)).

The subsequent evolution of the central vortex depends critically on the Burger number $B_{\text{core}} = N_c H / (fR)$, where $N_c = N(1 - 0.2B^{-1})^{1/2}$ is the buoyancy frequency of the central core following the establishment of the corner regions. For $B > 1.0$, the axisymmetry of the system is retained throughout the spin-up process: the central vortex attains a state of near solid body rotation by the diffusion of vorticity from the sidewalls. For $B < 1.0$, the central core becomes baroclinically unstable, and its streamlines strained from circles into ellipses. Subsequently, for $N_c/f < 1$ (and $B < 1.0$), the symmetry of the central core is broken in a manner reminiscent of the elliptical instability. For short tanks ($2H/R < 1$), the instability is marked by a simple tip-over of the central core in the laboratory frame that is resisted by the core stratification. For $2H/R > 1$, the centreline of the stratified core is deflected into a helical form before the core breaks into a series of stacked vortices. A Burger number criterion, $B = NH/(fR) < 1.0$, for the baroclinic instability of the central core is derived and found to be consistent with the experimental observations.

Keywords: Spin-up; Rotating fluids; Stratified fluid; Baroclinic instability; Elliptic instability; Vortex

1 INTRODUCTION

The adjustment of stratified fluid from one state of rotation to another arises frequently in various settings in both industrial and geophysical fluid dynamics. Spin-up is a term used to describe the adjustment of a fluid volume from one state of solid body rotation to another. An extensive review of spin-up in both homogeneous and stratified fluids is

*Corresponding author. E-mail: flor@hmg.ingp.fr

presented by Duck and Foster (2001). When the change in rotation rate is incremental, the mathematical formulation is greatly simplified as the governing equations become linear. The linear spin-up of a homogeneous fluid was described by Greenspan and Howard (1963) and Greenspan (1968), and is controlled exclusively by boundary layer transport. The case of nonlinear spin-up from rest of a homogeneous case is considerably more complex, but has been treated by Wedemeyer (1964) and Weidman (1976a,b). While considerable attention has been given to the problem of linear spin-up of a stratified ambient (Holton, 1965; Pedlosky, 1967; Buzyna and Veronis, 1971; Hewitt *et al.*, 1999), very little has been given to the related nonlinear problem.

Greenspan (1981) presented a short note reporting experimental observations of spin-up from rest of a stratified fluid bound in a cylindrical container. While parameter regimes were not delineated, both axisymmetric and asymmetric flow regimes were observed; moreover, both baroclinic and elliptical instabilities were identified. We here present the results of an experimental investigation of spin-up from rest of a stratified fluid, in which we extend and quantify the qualitative observations made by Greenspan (1981). Particular attention is given to delineating the criteria for stable axially symmetric spin-up and for the observed modes of axisymmetry-breaking instability.

An initially quiescent cylindrical tank of height $2H$ and radius R containing a stably stratified fluid with constant Brunt–Väisälä frequency N is impulsively set into motion at an angular speed $\Omega = f/2$. In a recent paper, the authors [Flor *et al.* (2002), hereafter FUB] present a combined experimental, numerical and theoretical investigation of the early stages of this process. The theoretical model represents an extension of that of Wedemeyer (1964) to the case of a stratified ambient, and yields good agreement with both experimental observations and numerical simulations. The authors demonstrate that an initial axisymmetric phase arises that is dominated by the generation of corner regions through radial boundary layer transport along the horizontal boundaries. After a time $\tau \sim 1.3(E^{1/2}N)$ where the Ekman number $E = \nu/(\Omega R^2)$, two distinct fluid domains thus emerge, the corner regions, and the central stratified core. After this initial stage, a substantial volume of non-rotating core fluid persists, shrouded from the container boundaries by buffer regions of rotating fluid. We here examine the stability of the initially axisymmetric configuration. We demonstrate that the subsequent evolution depends explicitly on N/f and H/R , and detail the nature of this dependence.

In Section 2, we review the physical processes accompanying the initial stage of spin-up marked by the development of the corner regions. The details of this process are worth our careful consideration, as they determine the ultimate stability of the core vortex. In Section 3, we describe the apparatus and procedure followed in our experimental study. Our experimental observations are detailed in Section 4. In Section 5, we consider the mechanism responsible for the axisymmetry-breaking instability. Specifically, we adapt the stability analysis of Griffiths and Linden (1981) in order to deduce a Burger number criterion for baroclinic instability of the central core. In Section 6, we summarize the results of our study.

2 DEVELOPMENT OF THE CORE VORTEX

The ultimate stability of the core flow is strongly influenced by the initial phase of spin-up from rest, detailed in FUB, and briefly reviewed here for the sake of clarity.

It is marked by the establishment of boundary layer flows which transport fluid radially outward along the upper and lower bounding surfaces and into corner regions whose height is limited by the stratification. The density of the fluid transported radially into the corner regions decreases progressively; consequently, the fluid is placed layerwise in the corner regions, where a radial stratification thus develops. The corner regions may either extend to the midplane of the tank, or fall short. In the former case, the central core loses contact with the sidewalls, while in the latter, vertical boundary layers develop through the diffusion of angular momentum from the sidewall. At the end of this initial stage, the flow is characterized by an isolated, stationary, vertically-stratified core region suspended between the rotating corner regions (Fig. 6(b)). The vertical stratification within the core is diminished by the vertical boundary layer transport forced in the initial stage (note the reduced number of horizontal dyelines from Fig. 6(a) and (b)).

According to the results obtained in FUB, fully developed corner regions have approximately a height $h = 0.3fR/N$ and volume

$$\Delta V = \frac{2}{3}\pi hR^2 = \frac{\pi}{5}R^3 \frac{f}{N}. \quad (1)$$

When the Burger ratio (the ratio of the Rossby deformation radius NH/f to the tank radius R), $B = NH/(fR) < 0.3$, the corner regions thus extend to the midplane of the tank, $h > H$. The development of the corner regions requires that the isopycnals within the central core be displaced by a vertical distance

$$\Delta z = \frac{\Delta V}{\pi R^2} = \frac{1fR}{5N}. \quad (2)$$

This vertical stretching necessarily decreases the density gradient within the core: the Brunt-Väisälä frequency is reduced to a value N_c given on the average by

$$N_c = N \left(1 - \frac{\Delta z}{H}\right)^{1/2} = N \left(1 - \frac{1}{5B}\right)^{1/2}. \quad (3)$$

The radius of the stationary core decreases slightly during the establishment of the corner vortices owing to the diffusion of vorticity from the sidewalls. The thickness ΔR of the sidewall boundary layers after the time required for the development of the corner vortices, $T = 1.3E^{-1/2}N^{-1}$, is given by

$$\frac{\Delta R}{R} = \left(1.3 \frac{\Omega}{N}\right)^{1/2} E^{1/4}. \quad (4)$$

In the parameter regime of interest to our experiments, the resulting change in the core radius is negligibly small, of order 10% or less.

When $B < 0.3$, the corner regions extend vertically to the midplane of the tank; consequently, the core will be entirely separated from the sidewall boundaries by spun-up fluid regions. The form of the central core region will thus depend explicitly on the aspect ratio of the cylindrical tank.

3 EXPERIMENTAL STUDY

A detailed description of the experimental apparatus and technique is given in FUB. We here reiterate the important points. Experiments were performed at two different sites, the Fluid Dynamics Lab at MIT and the LEGI in Grenoble. A schematic illustration of the experimental apparatus is presented in Fig. 1. Five cylindrical tanks, of inner diameter 14, 30, 44, 50, and 72 cm were used in the experiments. The tank was positioned on a 1.0-m diameter rotating platform and filled with a linearly stratified saltwater solution using the Oster double-bucket technique.

After the tank was filled, horizontal or vertical planes of fluorescein dye were enplaced in the fluid. The horizontal dye planes correspond to isopycnals, and their evolution reveals the vertical motion within the tanks. Horizontal planes were enplaced using a metal frame spanned by cotton strings coated with dried fluorescein dye

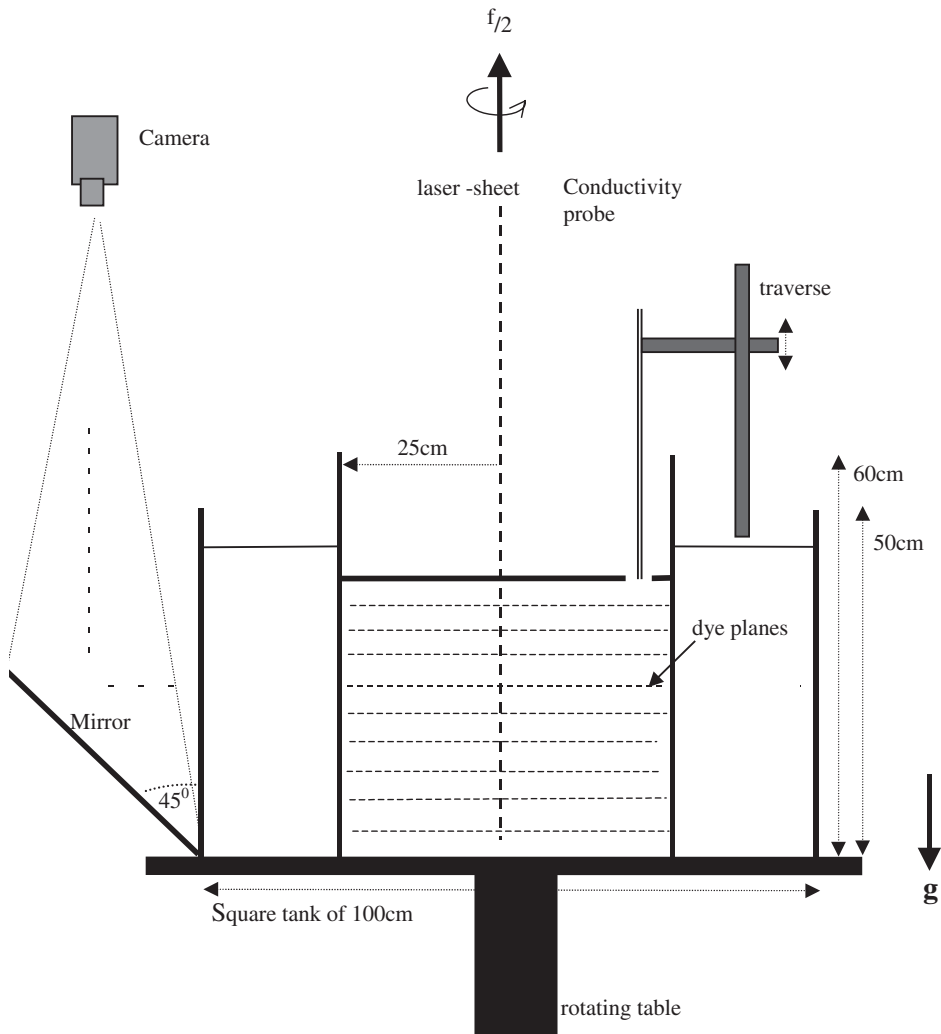


FIGURE 1 A schematic illustration of the experimental apparatus.

(Hopfinger *et al.*, 1991). The frame was removed and a horizontal lid placed on top of the tank. Vertical planes were emplaced by slowly sweeping a vertical dyed string (with a weight attached at its base) through the tank. Before the rotation was initiated, the vertical density profile was measured, by passing a conductivity probe vertically through the fluid domain and the Brunt–Väisälä frequency $N = [-(g/\rho)(\partial\rho/\partial z)]^{1/2}$ calculated. The table was set into motion, and the rotation frequency $f = 2\Omega$ achieved in less than one rotation period. The density profiles were measured several times during the spin-up process. The flow was illuminated by a vertical laser or light sheet which passed through the tank centreline. Observations of the dye field gave information about the boundary layer flows, the instability of the non-rotating core fluid, and a qualitative measure of the mixing of the stratified fluid. A digital camera mounted in the rotating frame (see Fig. 1) recorded the flow evolution and the images were directly recorded onto the hard disk of a PC.

The $(f/N, 2H/R)$ parameter regime was explored. The non-dimensional parameter ranges covered were $0 \leq N/f \leq 2.5$ and $0.54 \leq H/R \leq 3.5$, and the Ekman number was of the order $O(10^{-5})$. Five particular experiments will be discussed in detail.

4 EXPERIMENTAL OBSERVATIONS

The increase in vertical distance between the isopycnals within the stratified central core that accompanies the development of the corner regions is evident in Figs. 5–10. The evolution of the horizontal dye lines allows for the computation of the density gradient within the central core. In Fig. 2, we present the observed dependence of the density gradient within the central core following establishment of the corner regions.

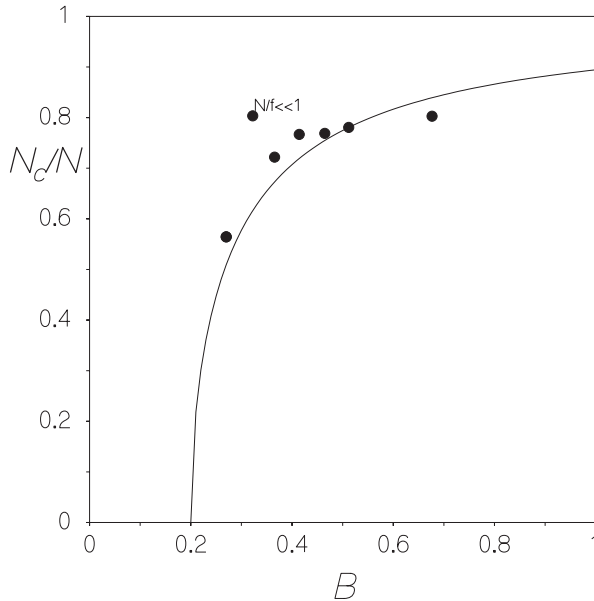


FIGURE 2 The core stratification following establishment of the corner regions. Experimental values are deduced from the vertical displacement of the horizontal dye lines (see e.g. Figs. 5a, b and 7a–d) and compared with (3).

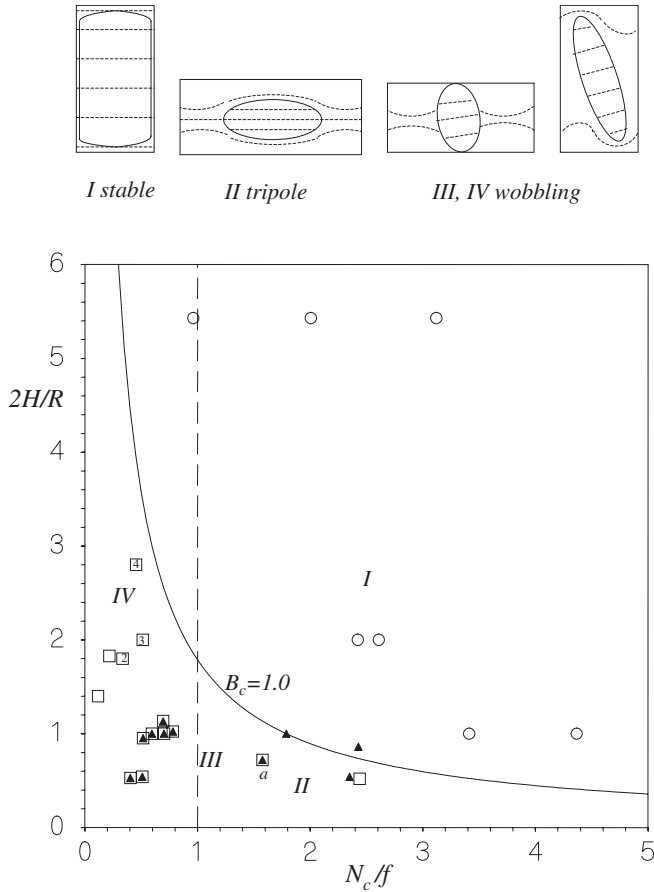


FIGURE 3 Schematics of the different regimes (above) and regime diagram (below) illustrating the dependence of the form of the flow on the governing parameters, specifically, the ratio of the core stratification to rotation rate, N_c/f , and the aspect ratio of the core vortex, $2H/R$. Open circles: stable vortices; triangle: tripolar vortices; open squares: wobbling vortex. In region IV the number of vortices into which the core vortex breaks up, is displayed within the squares. The criterion for instability, $B_c \leq 1.0$, is based on the initial Burger number $NH/(fR)$ and is therefore transformed to the axes represented in the figure to the criterion $2B_c\sqrt{1-1/(5B_c)} \leq 3.31$ for instability.

Specifically, we indicate the dependence of the percentage decrease in stratification on the Burger number, $B = NH/(fR)$. Our experimental data is evidently well described by Eq. (3).

The second stage of the flow evolution was observed to depend explicitly on the aspect ratio of the core, $2H/R$, and on N_c/f . The stratified spin-up regime diagram is presented in Fig. 3, and makes clear that several distinct flow regimes arise according to the values of the reduced Burger number B_{core} and N_c/f . These regimes are considered in turn below.

4.1 Axisymmetric Flows

In region I of Fig. 3, the flow maintains its axisymmetry throughout the spin-up process. Figure 4 illustrates a typical flow evolution in a case where the dye was initially

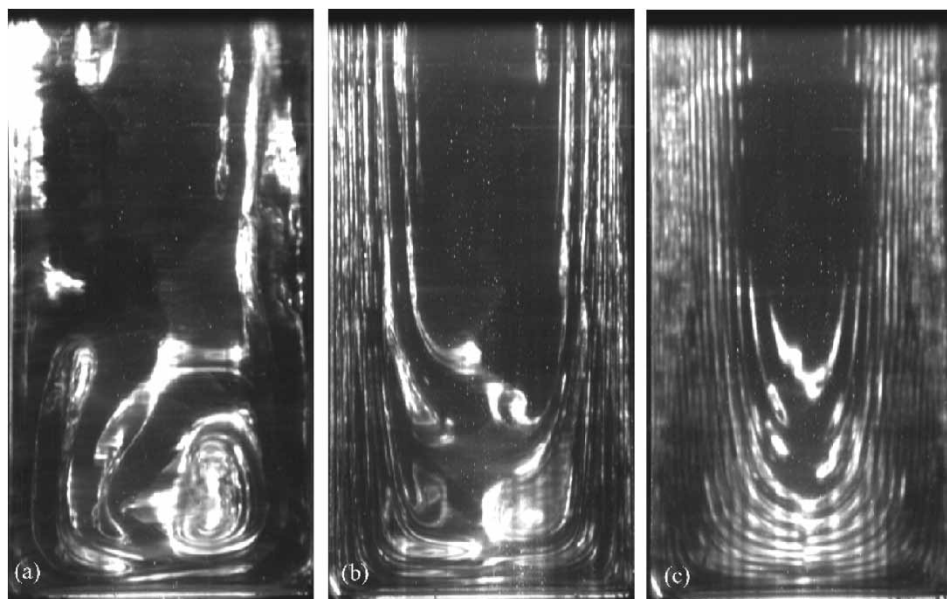


FIGURE 4 The evolution of the flow in the stable region I of the regime diagram (Fig. 3). (a) At $t=0$, just prior to initiating spin-up; (b) at $t=200$ s; (c) at $t=259$ s. Note the winding of the dye into an onion shaped structure by the rotational shear induced by the sidewall boundaries. Experimental parameters (exp 1 in Table I) with $N_c/f = 3.16 \text{ s}^{-1}$, $2H/R = 5.43$ and the tank radius is $R=7$ cm. Only the lower half of the tank is shown.

distributed along vertical lines. The initial spin-up stage is also represented in Fig. 5. The development of the corner regions results in the bowing of the isopycnals (see Fig. 5(b)). Following the establishment of the corner vortices, the corner fluid slowly slumps back horizontally owing to the diffusion of vorticity from the sidewalls: as the difference in angular velocity across the boundaries of the corner eddies is diminished, so too is the curvature of the isopycnals. Subsequently, the core fluid spins up principally by the viscous diffusion of momentum from the container boundaries. The final state of near solid-body rotation is thus achieved after a time $\tau \sim R^2/\nu$. The stratification thus serves to limit the spin-up process to a shallow layer through suppressing the vertical boundary layer transport that arises in the homogeneous system. We note that the final state is characterized by a three-layer structure: a stratified central layer bound above and below by the partially mixed fluid that once constituted the corner regions.

4.2 Asymmetric flows

In region II of Fig. 3, the axial symmetry of the flow is broken in a manner that depends explicitly on the value of N_c/f . A typical sequence for the parameter regime $N_c/f > 1$ and $2H/R < 1$ is shown in Fig. 6. After the establishment of the corner regions and the spin-up of the fluid near the sidewall boundaries, the mixed corner fluid slowly flushes back to the centre of the tank. Simultaneously, baroclinic waves propagate along the interfaces between interior and corner regions and the central core loses its symmetry. We denote by mode 1 a lateral shift of the corner region, and by mode 2 an elliptical deformation of the initially circular corner region. The mode 1 and 2

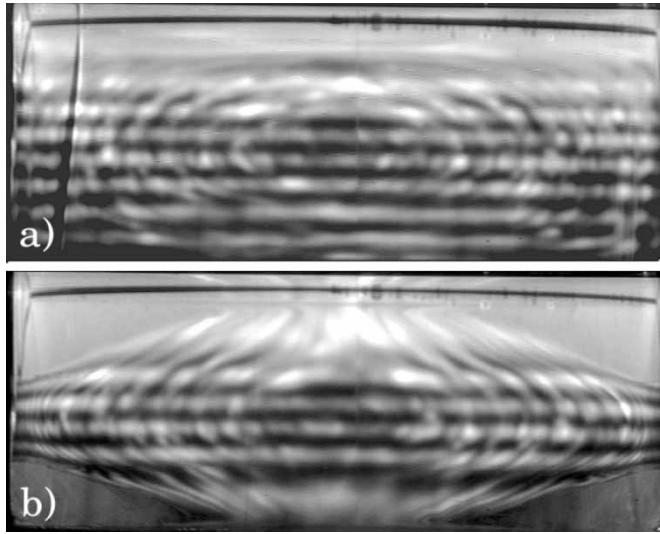


FIGURE 5 Initial stage of the spin-up showing the formation of the mixed corner regions and stationary core. At (a) $t=0$, just prior to initiating spin-up, and (b) $t=142$ s, after the maturation of the corner regions. Experimental parameters (exp. 20 in Table I): $N/f = 1.88 \text{ s}^{-1}$ and $2H/R = 0.72$; the tank radius is $R = 25$ cm.

TABLE I Governing parameters for experiments performed in the present study

<i>Exp.</i>	$2H$ (cm)	R (cm)	N (s^{-1})	f (s^{-1})	B	N_c/f	$2H/R$
1	38	7	1.43	0.453	8.57	3.12	5.43
2	38	7	1.43	0.7	5.54	2.01	5.43
3	38	7	1.43	1.43	2.71	0.96	5.43
4	30	15	1.01	0.4	2.53	2.42	2.0
5	30	15	1.41	2.26	0.62	0.51	2.0
6	30	15	1.41	0.52	2.71	2.61	2.0
7	42	15	1.21	2.28	0.74	0.45	2.8
8	21	15	0.74	2.26	0.23	0.12	1.4
9	27	15	1.05	2.26	0.42	0.34	1.8
10	17	15	1.18	1.32	0.51	0.70	1.13
11	15	15	0.96	0.21	2.29	4.37	1.0
12	15	15	1.0	0.5	1.0	1.79	1.0
13	15	15	0.76	0.21	1.81	3.41	1.0
14	19	36	1.4	0.5	0.74	2.39	0.53
15	19	36	1.4	1.5	0.25	0.40	0.53
16	19	36	1.18	2.52	0.12	–	0.53
17	19	36	1.4	0.5	0.74	2.39	0.53
18	25	25	1.69	2.04	0.41	0.60	1.0
19	25	25	1.72	1.85	0.46	0.70	1.0
20	18	25	1.56	0.83	0.68	1.58	0.72
21	23.8	25	1.77	2.12	0.37	0.59	0.95
22	21.5	25	1.63	0.61	1.15	2.43	0.86
23	13.5	25	2.1	2.1	0.27	0.51	0.54
24	45.7	25	0.67	1.9	0.32	0.22	1.82
25	25.6	25	1.7	1.7	0.51	0.78	1.02

waves are marked, respectively, by asymmetric and axisymmetric oscillations of the corner regions.

Figure 6 shows the flow evolution for a relatively low value of N/f (point *a* in Fig. 3). Here, mode 1 oscillations grow, followed by a slight wobbling and simultaneous

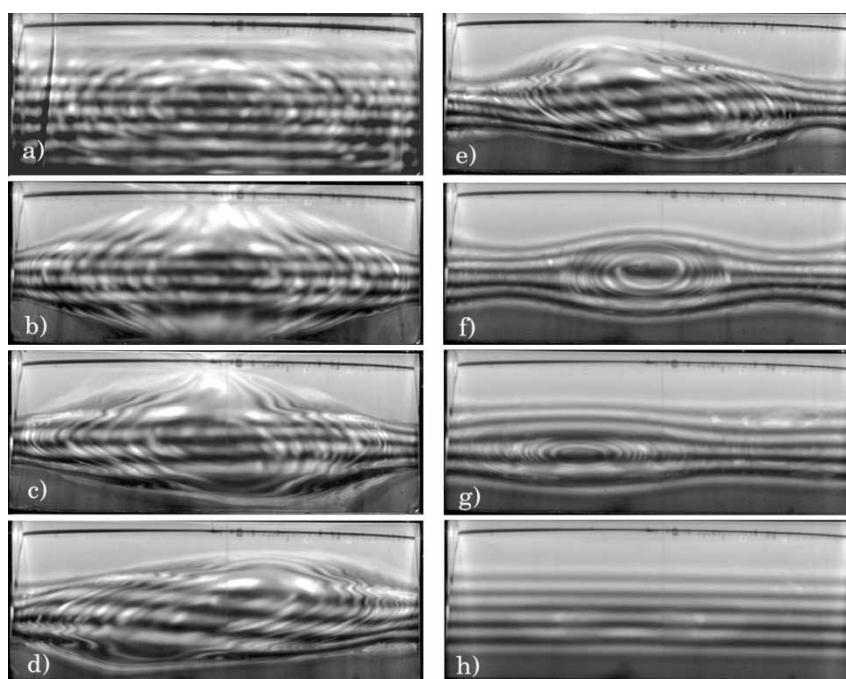


FIGURE 6 Core evolution in region II of the regime diagram (Fig. 3). At (a) $t=0$, just prior to initiating spin-up; (b) $t=142$ s, after the maturation of the corner regions; (c) $t=273$ s; (d) $t=361$ s; (e) $t=382$ s; (f) $t=616$ s and (g) $t=18$ min. The baroclinic waves along the corner interfaces are evident in (b), (c) and (d); the synchronized oscillations of the corner-regions suggest a mode 1 baroclinic wave. The wobbling of the core vortex is evident in (c), (d), (e) and (f), where the long and short side of the elliptical anti-cyclonic core vortex are apparent. The cyclonic satellite vortices are also evident in (f). Finally, (h) at $t=79$ min, the three remnant layers are apparent. Note that the initial circular dye structure evident at $t=0$ is a remnant from the initial dye emplacement. Experimental parameters (exp. 20 in Table I): $N/f = 1.88 \text{ s}^{-1}$ and $2H/R = 0.72$; the tank radius is $R = 25$ cm.

increase in ellipticity of the core region (see Fig. 6(c) and (d)). As the corner fluid flushes back to the centre, the near-wall rotating fluid is also stretched, inducing the formation of two cyclonic satellites which can be discerned from the vertical compression of the dye lines near the outer wall (see Fig. 6(c) and (d)) and together with the elliptical core comprise a tripolar vortex. In the subsequent evolution, the tilted core vortex abutts the sidewall and dissipates or even breaks up (not shown) thus reducing its size while the two satellites merge, leading eventually to an asymmetric dipolar vortex (see Fig. 6(g)). Throughout this flow evolution, the isopycnals within the central core and adjoining vortices are only weakly distorted from the horizontal. With increasing values of N/f and B , the baroclinic interfacial waves and core wobbling are reduced in amplitude and the evolution of the core into a tripolar vortex was weaker or even absent.

In Section 5, we shall demonstrate that the axisymmetry-breaking instability observed in this regime may be interpreted as a baroclinic instability understood by analogy with that described by Griffiths and Linden (1981).

When $N_c/f < 1$ (region IV in Fig. 3), the development of the symmetry-breaking baroclinic instability is accompanied by a tilting of the central core reminiscent of classic elliptical instability (Kerswell, 2002). Figure 7 shows the evolution in this case, and

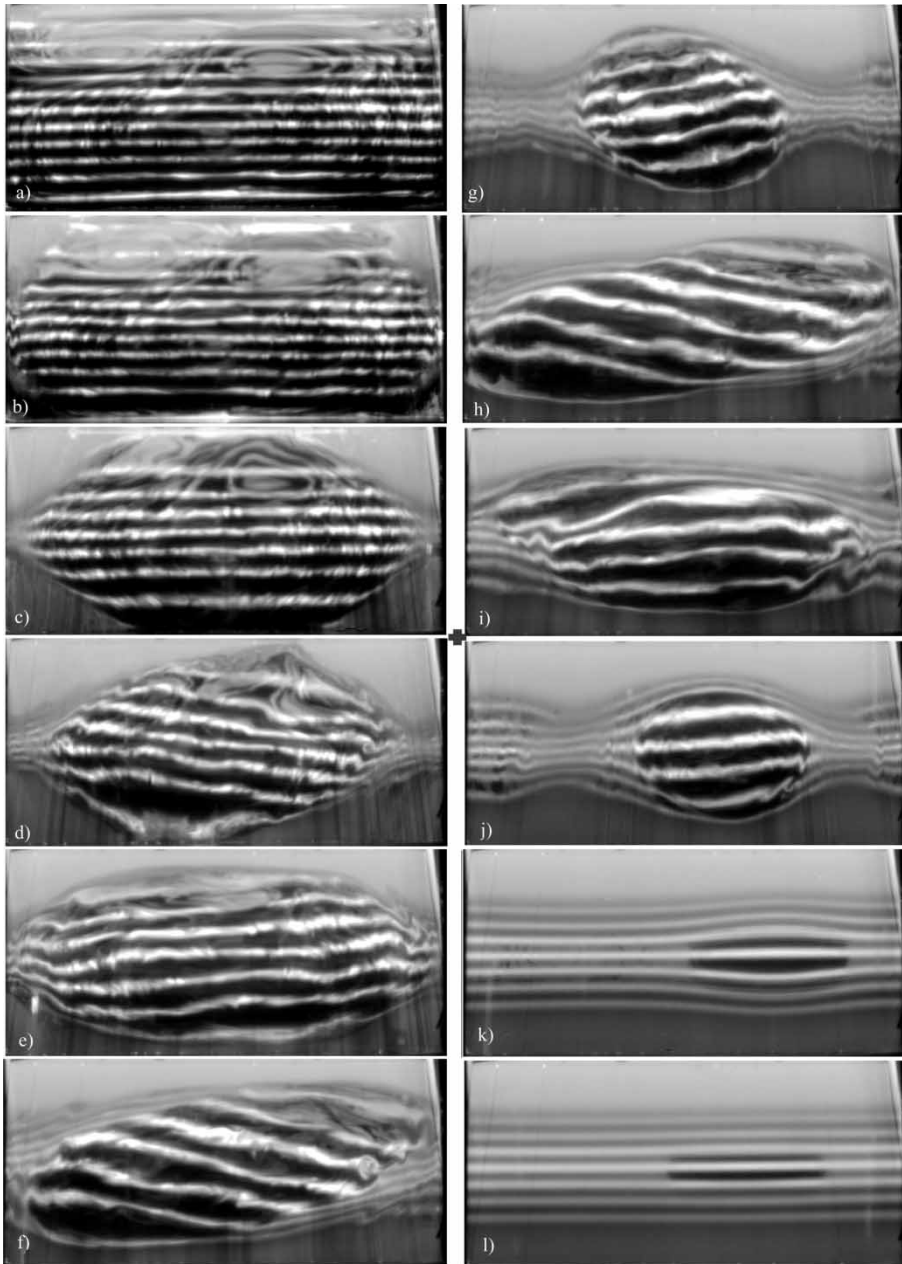


FIGURE 7 Core evolution in region IV of the regime diagram (Fig. 3). (a) At $t=0$, just prior to initiating spin-up. Unstable wave motion along the side-wall boundary (see Fig. 9) leads to the mixing evident at (b) $t=31$ s. After the formation of the corner regions, (c) 125 s the wobbling of the core region commences as is evident at (d) $t=189$ s. When the entire lower boundary is covered with rotating fluid (e) $t=210$ s, the core develops into an ellipsoid while the amplitude of the oscillation and the ellipticity of the core increase (f) $t=288$ s, (g) $t=294$ s, (h) 303 s. The long and short sides of the core are evident in, respectively, (e), (f), and (h) and (d), (g), and (j). The cyclonic satellite vortices are evident in (g) and (j). At its maximum ellipticity the core vortex becomes peanut-shaped and internal waves pinch off top and bottom, (i) 355 s, thus reducing the core size (j) 427 s. After dissipation of a dipolar remnant vortex (k) $t=188$ min, three layers emerge at (l) $t=200$ min. Experimental parameters (exp. 21 in Table I): $N/f = 0.84$, $2H/R = 0.95$, tank radius $R = 25$ cm.

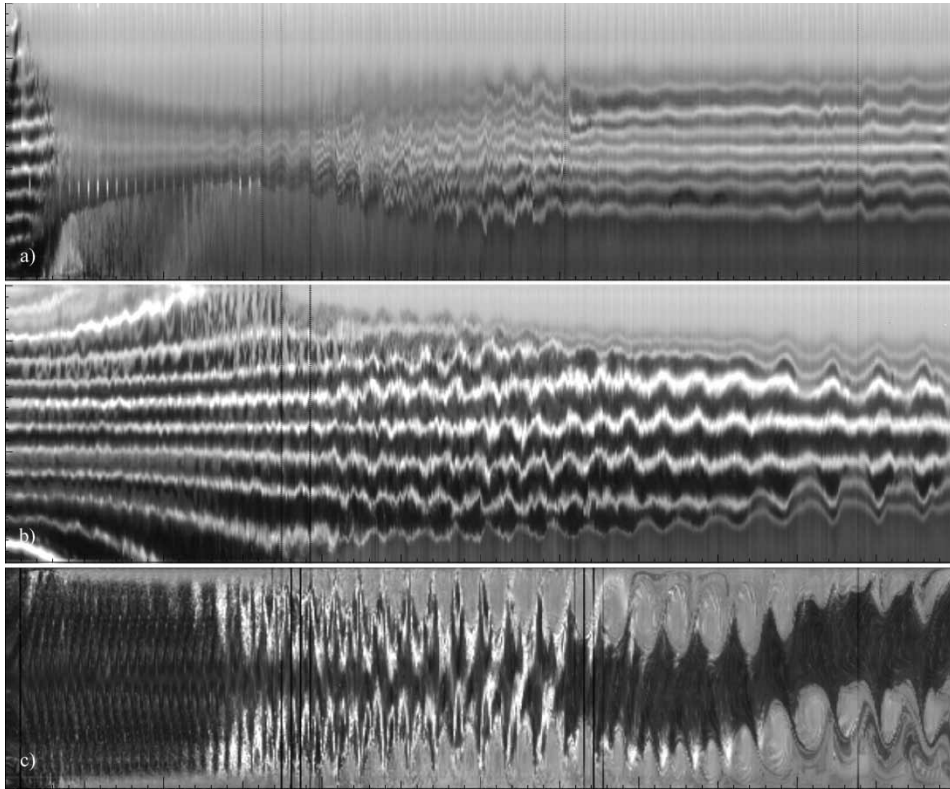


FIGURE 8 Spatio-temporal evolution of the dye along a vertical line at (a) the rim of the tank and (b) the centre of the tank for the experiment shown in Fig. 7. The vertical time bars along the horizontal axes denote 10 s intervals; the lines along the vertical axes indicate 1 cm intervals. (c) The evolution of the vortex over a horizontal mid-cross-section in time (horizontal axis) shows the simultaneous wobbling and rotation of the elliptical core vortex (dark regions) while for large t it shows the lateral advection of mixed fluid by the cyclonic satellite vortices (gray) near the boundary. The white peaks for $120 < t < 250$ correspond to the wobbling of the horizontal dye lines. Note that the core oscillation starts during the formation of the core region.

clearly illustrates both the ellipticity and the wobbling of the central vortex. The wobbling is in phase with the baroclinic waves at the interface of the corner region (as revealed by the time sequences in Fig. 8(a), (b) and (c)). Here, the central vortex interacts with the sidewall boundary (Fig. 7(e)–(i)) which leads to an inward propagating internal wave which prompts the break off of a small blob of fluid on top of the central vortex (Fig. 7(h) and (i)). The accompanying evolution of the isopycnals at two fixed radii is presented in Fig. 8 and reveals that the period of the core oscillations is close to the rotation frequency of the turntable, indicating that the central core wobbles in the rotating frame, but is stationary in the lab frame. The observed instability thus corresponds to the central core simply tipping over in the laboratory frame. Figure 8(c) shows the spatio-temporal evolution of a horizontal line of pixels, that reveals the baroclinic oscillations of the interface (modes 1 or 2) as well as the motion of the central vortex and cyclonic satellite vortices in time. For $T > 120$ s these oscillations are initially of mode 2 and subsequently ($T > 200$) of mode 1. After $t = 250$ s, the wobbling is damped out (Fig. 7(i)) and the tripolar vortex (with black core, and ‘white’ satellites)

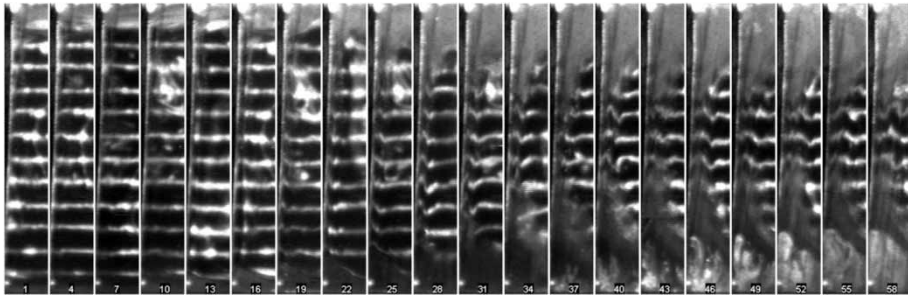


FIGURE 9 Sequence of images illustrating the amplification and eventual breaking of the wave motion near the sidewall of the tank for the experiment shown in Figs. 7 and 8. The length of the image covers the tank-height and is here 25 cm; the time intervals correspond to 3 s starting at $t=0$ s.

abuts the sidewall, thus advecting the vorticity from the sidewall and enhancing the spin-up process. Also in this parameter regime, a field of baroclinic waves is excited on the sides of the stratified core, as is evident in Fig. 9. These waves typically grow in amplitude until breaking, thus enhancing the mixing of the interior. The oscillations of the core regions and the wobbling of the interior start simultaneously at a later stage, as shown in Fig. 8(a), when the fluid from the corner regions is flushed towards the interior.

In taller tanks ($2H/R > 1$), the straining of the cigar-shaped central vortex into an ellipse leads to the helical deflection of the centreline of the central vortex in a manner again reminiscent of elliptical instabilities in tall tanks (Eloy, 2000). Subsequently, the central vortex breaks up into a number of vortices, the number increasing with the aspect ratio H/R of the tank (see Fig. 3).

A final case worth discussing is that of $B < 0.3$ (region III in Fig. 3), for which the corner vortices extend to the midplane of the tank, and so intrude towards the centre of the tank (see Fig. 10(a)–(e)). Nevertheless, the buoyancy frequency in the interior, N_c , corresponds well to the predicted value (3) (see Fig. 2). Following the maturation of the corner regions, the central core becomes elliptical, then proceeds to wobble and precess around the rotation axis (see Fig. 10(e) and (f)). Once again, the cyclonic satellite vortices are evident from the squeezed dyelines. The precession is clear in Fig. 10 for the case where the corner regions extend to the mid-plane of the tank. The wobbling is similarly evident in the marked deflection of the isopycnals from the horizontal as illustrated in Fig. 11. The wobbling of the central vortex may lead to its instability and break-up: the resulting secondary vortices are evident in Fig. 10(f)–(i).

5 STABILITY

Our observations reveal that the instability of the core region is initiated by the development of a baroclinic instability at the interface between the interior and corner regions, and that the resulting strain on the core flow may prompt an elliptical instability of the central core. We proceed by deducing a criterion for the baroclinic instability of the system.

The interior is stratified and quiescent, while the corners are homogenized and rotating. For the sake of simplicity, we examine the stability of an interface between two

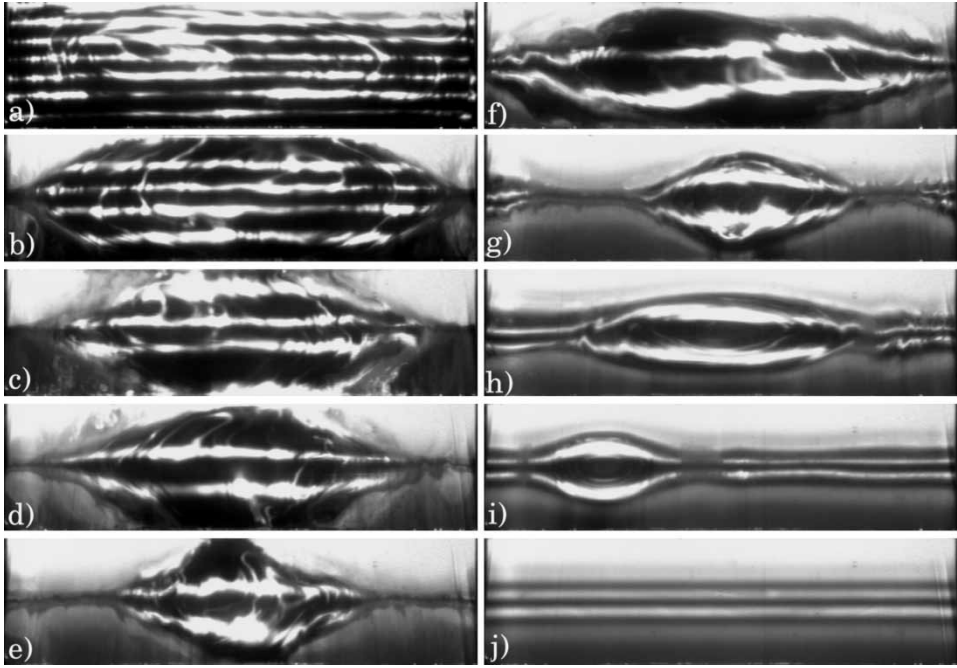


FIGURE 10 Flow evolution in region III of the regime diagram (Fig. 3) for the case where the corner regions span the entire depth of the fluid. At (a) $t=0$, just prior to initiating spin-up; (b) $t=67$ s, after the initial formation of the corner regions; at (c) $t=112$ s and (d) $t=159$ s, one observes their continuing growth due to the limited height of the tank. Subsequently, the core develops into an ellipsoidal form: at (e) $t=180$ s and (f) $t=188$ s, the short and the long side of the elliptical core are apparent, respectively. The cyclonic satellite vortices are apparent in (g) $t=233$ s and (h) $t=244$ s. After dissipation of the vortices, three layers emerge and are apparent in (j) $t=2$ h 48 min. Experiment parameters (exp. 23 in Table I): $N/f = 1$, $2H/R = 0.53$; the tank radius $R = 25$ cm.

homogeneous layers with uniform horizontal velocities (see Fig. 12). Specifically, we follow the approach of Griffiths and Linden (1981) who examined the baroclinic instability of the flow forced by the release of buoyant fluid from an annular source at the surface of a rotating fluid. We identify the interface between core and corner regions with their outer interface, and so readily adapt their analysis to examine the stability of our system. In our system, we assume that boundary layer transport is confined to the interface and negligible on the horizontal boundaries, an assumption expected to be valid provided the corner regions are spun-up.

Following Griffiths and Linden (1981), we eliminate the cylindrical geometry by considering the stability of a channel flow in a quasi-two-dimensional geometry. We take the dimensionless perturbation equations for the streamfunction ϕ defined relative to the rotating frame of reference with indices 1 and 2 denoting, respectively, the corner and interior regions:

$$\left(\frac{\partial}{\partial t} + U_1 \frac{\partial}{\partial x}\right) [\nabla^2 \phi_1 - F_1(\phi_1 - \phi_2)] - F_1 U_1 \frac{\partial \phi_1}{\partial x} = -\frac{E_1^{1/2}}{\epsilon} \nabla^2 \phi_1, \quad (5)$$

$$\left(\frac{\partial}{\partial t} + U_2 \frac{\partial}{\partial x}\right) [\nabla^2 \phi_2 - F_2(\phi_1 - \phi_2)] + F_2 U_2 \frac{\partial \phi_1}{\partial x} = -\frac{E_2^{1/2}}{\epsilon} \nabla^2 \phi_2, \quad (6)$$

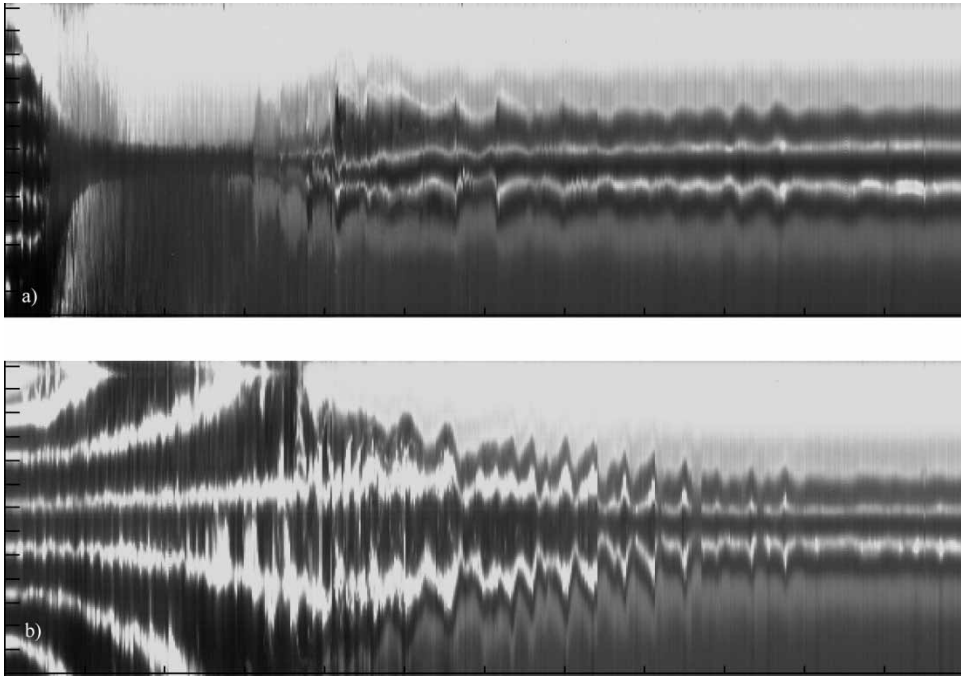


FIGURE 11 Spatio-temporal evolution of the dye along a vertical line at (a) the rim of the tank and (b) the centre of the tank for the experiment shown in Fig. 10. The vertical time bars along the horizontal axes denote 50 s intervals; the horizontal lines along the vertical axes indicate 1 cm intervals.

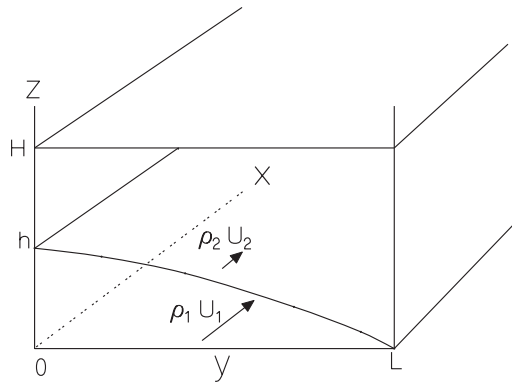


FIGURE 12 Schematic illustration of the model geometry and parameters.

where the Ekman numbers $E_1 = \nu/(\Omega h^2)$, $E_2 = \nu/[\Omega(H - h)^2]$, the Rossby number $\epsilon = u/(\Omega L)$, and L and h are, respectively, the width and mean height of the corner region and u is the characteristic velocity scale at the interface. As a typical velocity scale u we employ the mean velocity $\Omega R'$ where $R' = 2R/3$ is the middle of the corner region. The dimensionless velocities are $U_2 = -1$ and $U_1 = 0$, whereas the Rossby number $\epsilon = -(R'/L)$.

The Froude numbers are defined in Griffiths and Linden (1981) as $F_1 = f^2 L^2 / (N^2 H h)$ and $F_2 = f^2 L^2 / [N^2 H (H - h)]$, with $N^2 H = g / \bar{\rho} (\delta \rho / 2)$ and $\delta \rho$ the maximum density difference between mid-height H and tank bottom. Note that this is the maximum possible density difference across the interface. The radial extent and maximum height of the fully developed corner regions were calculated by FUB to be, respectively, $L = 2R/3$ and $h_{\max} = fR/(3N) = H/(3B)$. For the mean height we take the approximate value $h = h_{\max}/2$. We can thus express the Froude numbers for our system as $F_1 = 8/(3B)$ and $F_2 = (8/(3B))(1/(6B - 1))$ and the Rossby number as $\epsilon = -1$. Moreover, the depth ratio $\gamma = h/(H - h)$ is uniquely prescribed by B : $\gamma = 1/(6B - 1)$. By this definition of the Froude number, the Burger number is thus limited to $B = 1/6$, the value for which the corner region reaches mid-depth, i.e. $h = h_{\max}/2 = H$.

We follow Griffiths and Linden (1981) in considering perturbations of the form $\phi \sim \exp[ik(x - ct)] \cos ly$ with wave vector $K^2 = k^2 + l^2$ with cross-stream wave number $l = \pi/2$. A discussion of the dependence of the system on γ is presented in Griffiths and Linden (1981). Substituting the perturbations into (5) and (6) yield a dispersion relation

$$\alpha c^2 + \beta c + \Gamma = 0, \tag{7}$$

where

$$\begin{aligned} \alpha &= K^2 \left[K^2 + \frac{8}{3(6B - 1)B} + \frac{8}{3B} \right], \\ \beta &= \frac{6\sqrt{E}Pr}{\epsilon} K^2 \left[-\frac{16U'_2}{3B} - \frac{16U'_1}{3(6B - 1)B} - (U'_1 + U'_2)K^2 + I \frac{2(9K^2 B^2 + 8)}{3(6B - 1)Bk} \right], \\ \Gamma &= \frac{36EP^2}{\epsilon^2} K^2 \left(U'_1 K^2 U'_2 + \frac{8U'l^2}{3(6B - 1)B} + \frac{8U'^2_2}{3B} \right. \\ &\quad \left. - I \frac{\{[18U'_2 B^2 + 3(-U'_2 + U'_1)B]K^2 + 8(U'_2 + U'_1)\}}{6(6B - 1)Bk} - \frac{K^2}{4(6B - 1)k^2} \right). \end{aligned}$$

We have used the transformation $U'_i = U_i \epsilon / (6\sqrt{E}Pr)$; $E = \nu / \Omega R^2$ is the general Ekman number based on tank radius and $Pr = N/f$ is the Prandtl ratio. The shear across the interface is then $U'_1 - U'_2 = 1/(6\sqrt{E}Pr)$ and marginally stable conditions (zero growth rates) are obtained for

$$\frac{1}{6\sqrt{E}Pr} = \frac{(9K^2 B^2 + 8)K}{2\sqrt{1024 - (324B^4 - 108B^3 + 9B^2)K^6 - (192 - 1152B)K^2\sqrt{K^2 - l^2}}}. \tag{8}$$

The marginal stability curves for different B numbers are plotted as a function of the scaled wave number $K^2 B$ in Fig. 13(a). A minimum shear is evidently required for instability. The region of instability is bounded on either side: for a fixed Burger number B , the lower bound is set by viscous dissipation of the long waves via Ekman layer friction (at left in Fig. 13(a)), while the short-wave cut-off (at the right in Fig. 13(a)) corresponds to the standard inviscid result for baroclinic instability

(Phillips, 1954; Pedlosky, 1970). The minimum of the marginal stability curves indicates the critical wave number k_m for which the flow first becomes unstable. The azimuthal wave number is $k_m \equiv L 2\pi/(\lambda_m)$ with $\lambda_m = 4\pi R/(3n)$ the mean circumference of the corner region, n the wave mode and $L = 3/2R$ the width of the current. With these scalings the mode n is equal to k_m . The most unstable azimuthal wave numbers are represented against B in Fig. 13(b) showing that the dominant modes of instability of the interface in the spin-up flow are mode 2 (elliptical) and mode 1 (circular). Schematic illustrations of these dominant modes are presented in Fig. 13(b). To interpret these results, it is helpful to consider the growth rate of the two modes for typical Ekman number and Prandtl ratio shown in Fig. 13(c). We note that, for small Burger number $B \leq 0.5$ mode 2 is the first unstable (see Fig. 13(b)), but since mode 1 grows the fastest it will eventually dominate, whereas for $B > 0.55$ mode 1 dominates as the first mode as well as the fastest growing mode. Further we note that the inverse B number is linearly proportional to the height of the corner region so that the theoretical outcome is very sensitive to the mean height of the corner region, $h_{\max}/2$.

The critical Burger number above which the flow is stable to all baroclinic perturbations can be found by setting the denominator in (8) to zero. For $K = l = \pi/2$, one thus finds $B_c = 1.00$. The corresponding line is represented in Fig. 3, where the $B = NH/(fR)$ number is calculated from the initial value for N (since the value of h_{\max} depends on N and not N_c). This critical Burger number represents the left side in Fig. 13(b), corresponding to long waves (small k) implying the possible growth of the lowest modes for $B < B_c$. There is a cut-off at $B < 1/6$, where the ratio γ vanishes. Since the layers have equal depth, we assume $\gamma = 1$ (and thus $F_1 = F_2$, $E_1 = E_2$), and so obtain

$$\frac{1}{6\sqrt{E}Pr} = \frac{\sqrt{3}\sqrt{B}K}{\sqrt{(16 - 3K^2B)(K^2 - l^2)}}. \quad (9)$$

The most unstable wavelength and vertical shear are thus given by

$$k_m = \left(\frac{144l^2}{B}\right)^{(1/4)} \quad \text{and} \quad \frac{1}{6\sqrt{E}Pr} = \frac{2(27l^2B^5)^{1/4}}{\sqrt{(4 - \sqrt{3}l^2B)(4\sqrt{3}l^2B^3 - 3l^2B^2)}}. \quad (10)$$

All flows with $B > 64/(3\pi^2) = 2.16$ are stable. The minimum B value for which baroclinic modes are predicted to arise are also presented in Fig. 3 along with our experimental observations. In accordance with the predictions of the stability theory, spin-up flows with Burger number smaller than the critical B_c number are generally found to be unstable.

In all experiments we found that wave mode 1 dominates the motion at the interface of the corner region. For low Burger number, initially a mode 2 can be discerned from the oscillatory motions at the interface (see Fig. 8(c)) in agreement with the theory represented in Fig. 13(b). Nevertheless, a mode 1 eventually grows and dominates in agreement with the predicted higher growth rate of this mode (see Fig. 13(c)). Also, the growth in perturbation amplitude, being slow for $B > 0.8$ and large for $B < 0.6$ is in agreement with the theoretical predictions. The observations are consistent with

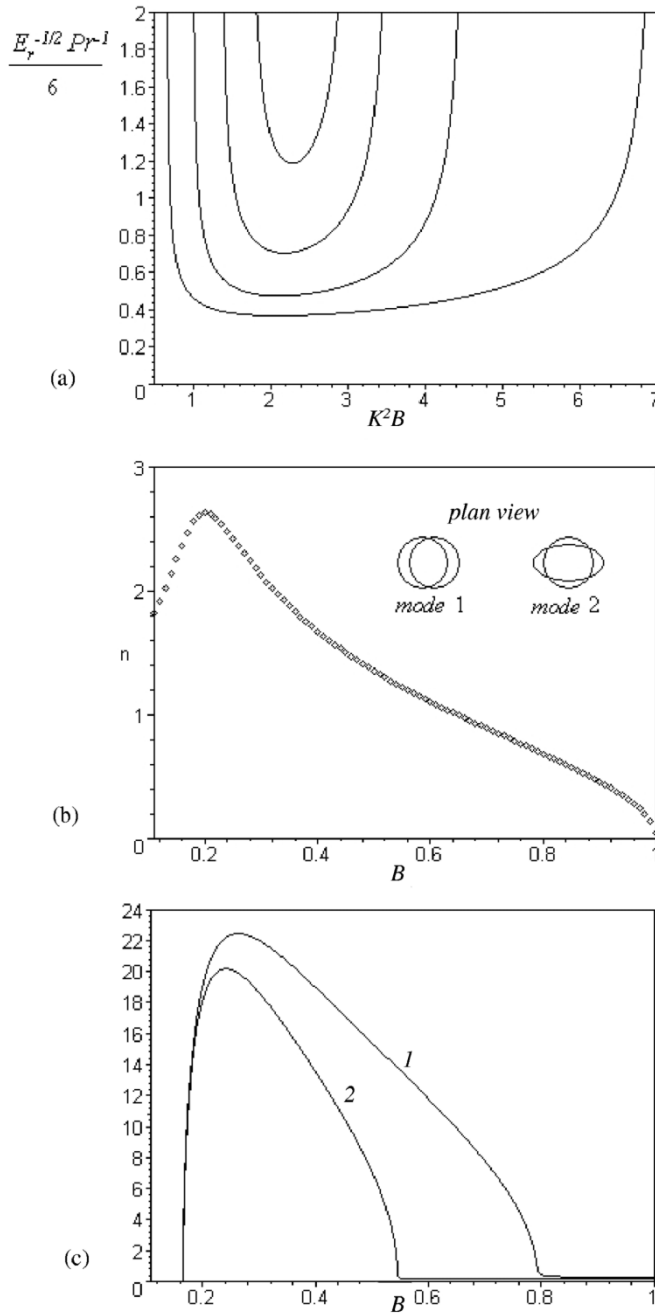


FIGURE 13 (a) Marginal stability curves calculated from (8) for Burger numbers $B = 0.265, 0.40, 0.55$ and 0.70 using Maple V. The minimum of each curve represents the minimum wave number $k_m = (K^2 - Pi^2/4)^{1/2}$ for which the flow becomes unstable for a specific value of the shear $1/(6E^{1/2}Pr)$ and (b) these first-unstable wave numbers presented as a function of Burger number. In (c), the growth speeds of wave number 1 (upper curve) and 2 (lower curve) are represented against Burger number B for $1/(6E^{1/2}Pr) = 52$, a good approximation to the present experiments for which $E \sim O(10^{-5})$ and $Pr = 1$ (higher modes have smaller growth rates). A schematic illustration of the mode 1 and 2 wave instabilities is displayed in Fig. 13(b).

the theoretical result, and so support the hypothesis that baroclinic instability is the mechanism responsible for the asymmetric flows observed.

6 DISCUSSION

The evolution of the initial stage of non-linear spin-up from rest of a stratified fluid, specifically the development of the corner regions and persistence of a stratified central core, was detailed in FUB. Our experiments have revealed that the subsequent evolution of the flow depends critically on the structure of the non-rotating core, specifically, its aspect ratio $2H/R$ and f/N_c , where N_c denotes the buoyancy frequency within the core established by the initial stage of spin-up. The geometry of the core region is prescribed by that of the corner regions, and the buoyancy frequency within the core $N_c = N(1 - 0.2B^{-1})^{1/2}$ reflects the degree of stretching of isopycnals by the vertical transport into the horizontal boundary layers. The subsequent evolution of the stratified core has been interpreted in terms of the combined influence of baroclinic and elliptical instabilities of the central core.

For $B > 1.0$, the core remains stable and the system maintains its axisymmetry throughout the spin-up process, which occurs on a diffusive timescale. Ultimately, the fluid is thus characterized by three layers, remnants of the mixed top and bottom corner regions and the stratified core (Greenspan, 1981). For $B < 1.0$, the interface between the stratified central core and homogenized corner regions becomes baroclinically unstable. Our experiments and theoretical developments indicate the dominance of an interfacial wave mode 1 disturbance in the parameter regime examined; this wave has a maximum growth-rate for approximately $B < 1.0$ above which we note that the wobbling does not occur. The onset of instability of the central core has been interpreted in terms of a baroclinic instability that develops at the edges of the corner regions. The Burger number criterion for instability, $B < 1.0$, was found by adapting the theoretical developments of Griffiths and Linden (1981), and is consistent with our experimental observations. The agreement of the theory with the data supports the hypothesis that baroclinic instability is the responsible mechanism.

The interfacial wave mode 1 (that increases in amplitude with decreasing N_c/f), is presumably related to the wobbling of the core region. The accompanying upward motion of the corner regions applies a baroclinic torque on the interior, and suggests an opposite tilt of the interior isopycnals as observed. When this mode develops at the interface, the swirling circular motion of the central core (relative to the rotating frame) is subjected to a straining motion that may prompt an elliptical instability. For $N_c/f < 1$, the core develops an elliptical instability very similar to those observed by Malkus (1989) and Eloy *et al.* (2000). While in their experiments, elliptical instability was prompted by boundary forcing, that is by deforming a rotating cylinder into an ellipse, in our experiments the elliptical straining is forced by the baroclinic instability of the central core.

In a short container ($2H/R < 1$), the instability is marked by the tipover of the central core reminiscent of the elliptical tipover mode elucidated by Waleffe (1990) as resulting from the interaction of a horizontal vorticity perturbation and the background strain. In a tall container ($2H/R > 1$), the centreline of the central core was initially distorted into a helix in a manner reminiscent of the homogeneous experiments of Eloy (2000). Subsequent interaction with the sidewalls generally lead to the break-up

into different lenses. For increased values of rotation, $N_c/f \ll 1$, the wobbling is reduced and an elliptical, cigar-shaped vortex precesses around the rotation axes. The instabilities in this case were marked by the distortion of the core streamlines into ellipses, and the subsequent instability of the stratified core to elliptical instabilities (Kerswell, 2002). The flow ultimately resumed an axially symmetric form and spin-up continued by diffusion, mainly from the sidewalls.

A number of caveats should be made concerning our stability analysis. First, the theory is based on the quasi-geostrophic ($\epsilon \ll 1$) vorticity equations while the present flow is more accurately ageostrophic ($\epsilon = -1$). At the end of the spin-up of the boundaries one can consider the interior flow as an anti-cyclonic vortex with vorticity $-f$ embedded in a rotating fluid and with an aspect ratio determined by the initial conditions. Though the stability of stratified vortices is discussed extensively in the literature, the non-linear stability of anti-cyclonic vortices has not yet been investigated and is left as a subject of future consideration.

Second, our analysis focusses only on baroclinic instability, thus implicitly assuming that the destabilizing shear is mainly vertical. In reality, both vertical and horizontal shear are present and either may trigger instability; if the horizontal shear is dominant, the instability is barotropic. The relative magnitudes of the two shears in the spin-up flow is prescribed by the slope of the interface, and so proportional to the $h_{\max}/L = \Omega/N$.

The flow evolutions shown in Figs. 6, 7 and 10 with the appearance of elliptical vortex structures and their subsequent tip-over remind us of elliptic instability and the instability driven by precession (see Kerswell, 2002). But, the growth-rates of the elliptic and precession instabilities are both proportional to the ellipticity of the flow, and so are initially zero in our spin-up flows. Furthermore, the relatively strong stratification and the zero absolute vorticity of the core are stabilizing (see Craik, 1989; Kerswell, 2002). These instability mechanisms will be effective when the baroclinic waves that distort the flow axisymmetry couple with inertial waves and thus enhance elliptical instability and/or precession driven instability.

In this respect it is worth noting that our critical Burger number is of the same order as the minimum critical Burger number found by Miyazaki and Hanazaki (1994) for the baroclinic instability of elliptical and circular vortices in a rotating stratified fluid. Their circular vortices are unstable due to the resonant interaction between bending waves (which in the spin-up experiments can be interpreted as the wobbling due to large amplitude baroclinic waves of mode 1) and the elliptic deformation of the core vortex.

In the limit of small N/f , which corresponds to mainly barotropic shear, the bending mode dominates, and the flow evolves in a manner reminiscent of the elliptical instability observed by Eloy *et al.* (2000) in homogeneous flows. An interesting extension of the current study would be an investigation of the influence of weak stratification on the elliptical instability observed by Eloy (2000).

Acknowledgements

JBF acknowledges Pierre Carecchio for his technical assistance in setting up the experiments and laser sheet. JWMB thanks Bev Thurber for her assistance with the experiments. The research was supported by NATO Linkage Grant MED.LG 974238 and by the Fund for Promotion of Research at the Technion.

References

- Buzyna, G. and Veronis, G., “Spin-up of a stratified fluid: theory and experiment”, *J. Fluid Mech.* **50**, 579–608 (1971).
- Craik, A.D.D., “The stability of unbounded two- and three-dimensional flows subject to body forces: some exact solutions”, *J. Fluid Mech.* **198**, 275–292 (1989).
- Duck, P.W. and Foster, M.R., “Spin-up of homogeneous and stratified fluids”, *Annu. Rev. Fluid Mech.*, **33**, 231–263 (2001).
- Eloy, C., “Instabilité multipolaire de tourbillons”, PhD thesis. Université Aix-Marseille II (2000).
- Eloy, C., Le Gal, P. and Le Dizès, S. “Elliptic and triangular instabilities in rotating cylinders”, *J. Fluid Mech.* **476**, 357–388 (2000).
- Flór, J.B., Ungarish, M. and Bush, J.W.M., “Spin-up from rest of a stratified fluid: boundary flows”, *J. Fluid Mech.* **472**, 51–82 (2002).
- Greenspan, H.P., *The Theory of Rotating Fluids*, Cambridge University Press (1968).
- Greenspan, H.P., “A note on the Spin-up from rest of a stratified fluid”, *Geophys. Astrophys. Fluid Dyn.* **15**, 1–5 (1981).
- Greenspan, H.P. and Howard, L.N., “On a time dependent motion of a rotating fluid”, *J. Fluid Mech.* **17**, 385–404 (1963).
- Griffiths, R.W. and Linden, P.F., “The stability of buoyancy-driven coastal currents”, *Dyn. Atmos. Oceans* **5**, 281–306 (1981).
- Hewitt, R.E., Davis, P.A., Duck, P.W. and Foster, M.R., “Spin-up of stratified rotating flows at large Schmidt number: experiment and theory”, *J. Fluid Mech.* **389**, 169–207 (1999).
- Holton, J.R., “The influence of viscous boundary layers on transient motion in a stratified rotating fluid, Part I”, *J. Atmos. Sci.* **22**, 402–411 (1965).
- Hopfinger, E.G., Flór, J.B., Chomaz, J.M. and Bonneton, P., “Internal waves generated by a moving sphere and its wake in a stratified fluid”, *Experiments in Fluids* **11**, 255–262 (1991).
- Kerswell, R.R., “Elliptical instabilities”, *Annu. Rev. Fluid Mech.* **34**, 83–113 (2002).
- Malkus, W.V.R., “An experimental study of the global instabilities due to the tidal (elliptical) distortion of a rotating elastic cylinder”, *Geophys. Astrophys. Fluid Dynam.* **48**, 123–134 (1989).
- Miyazaki, T. and Hanazaki, H., “Baroclinic instability of the Kirchhoff’s elliptical vortex”, *J. Fluid Mech.* **261**, 251–271 (1994).
- Pedlosky, J., “The spin-up of a stratified fluid”, *J. Fluid Mech.* **28**, 463–479 (1967).
- Pedlosky, J., *Geophysical Fluid Dynamics*, 624pp., Springer Verlag, New York (1970).
- Phillips, “Energy transformations and meridional circulations associated with simple baroclinic waves in a two-level, quasi-geostrophic model”, *Tellus* **6**, 273–286 (1954).
- Waleffe, F.A., “On the three-dimensional instability of strained vortices”, *Phys. Fluids* **76–80** (1990).
- Wedemeyer, E.H. “The unsteady flow within a spinning cylinder”, *J. Fluid Mech.* **20**, 383–399 (1964).
- Weidman, P.D., “On the spin-up and spin-down of a rotating fluid, I. Extending the Wedemeyer model”, *J. Fluid Mech.* **77**, 685–708 (1976a).
- Weidman, P.D., “On the spin-up and spin-down of a rotating fluid, II. Measurements and stability”, *J. Fluid Mech.* **77**, 709–735 (1976b).